Reversible modulation and ultrafast dynamics of terahertz resonances in strongly photoexcited metamaterials

I. Chatzakis, L. Luo, J. Wang, N.-H. Shen, T. Koschny, J. Zhou, and C. M. Soukoulis

Phys. Rev. B **86**, 125110 — Published 7 September 2012

DOI: 10.1103/PhysRevB.86.125110

Reversible modulation and ultrafast dynamics of THz resonances in strongly photoexcited metamaterials

I. Chatzakis,[1] L. Luo,[1] J. Wang,[1,*] N.-H. Shen,[1,†] Th. Koschny,[1] J. Zhou,[2,‡] and Costas M. Soukoulis[1,3]

[1] *Ames Laboratory and Department of Physics and Astronomy, Iowa State University, Ames, Iowa 50011, U.S.A.*

[2] *Center for Integrated Nanotechnologies, Los Alamos National Laboratory, Los Alamos, New Mexico 87545, USA.*

[3] *Institute of Electronic Structure and Laser, FORTH, 71110 Heraklion, Crete, Greece*

(Dated: August 20, 2012)

We demonstrate an ultrafast reversible modulation of resonant terahertz (THz) response in *strongly photoexcited* metamaterials. The transient spectral-temporal response of the dipole transition ∼1.6 THz exhibits a distinct non-monotonic variation as a function of pump fluence. The transition energy shift, strength, spectral width, and density-dependent ultrafast relaxation manifest a remarkable re-emergence of the transmission dip after initial quenching. Our simulations, incorporating the first-order diffraction from the photoinduced transient grating, reproduce the salient features, providing a new avenue for designing nonlinear and frequency-agile THz modulators.

PACS numbers: 78.67.Pt, 78.20.-e, 78.47.-p, 42.25.Bs

I. INTRODUCTION

Artificially subwavelength structured materials, so-called metamaterials,[1–4] attract strong current interest due to their exceptional properties, such as simultaneously negative permittivity $\varepsilon(\omega)$ and permeability $\mu(\omega)$, which imply a negative refractive index[1–5] not available in natural materials. In addition, artificial magnetism,[6,7] super focusing,[8,9] and specifically-tailored structures responding to ultra-broadband electromagnetic radiation from gigahertz (GHz), terahertz (THz), to visible range,[4,10] set them among the most promising candidates for next generation optoelectronic devices and large-scale photonic functional systems.

Recently, there has been significant interest in understanding ultrafast THz responses of nonlinear metamaterials, e.g., split ring resonators (SRRs) patterned on substrates exhibiting substantial nonlinearities.[11] The resulting components and schemes allow for constructing controllable active THz devices with dynamical tunability of amplitude and phase, which fills the demanding THz technology gap. Prior experiments using time-domain THz spectroscopy have demonstrated dynamic tuning of both magnetic[12–17] and electric[18] dipole resonances of SRRs on semiconductors or superconductors. More complex structures of coupled resonators on GaAs substrates have been proposed and experimentally studied, revealing frequency-agile THz modulation, e.g., a resonance shift with increasing photoexcitation.[14,16] However, thus far all ultrafast studies of THz materials have been concentrated on the relatively low photoexcitation, where a *reduction* or *quenching* of the resonant absorptions is observed.[13,14,19] Two outstanding issues are still poorly understood: first, there lack insights on how *high density* photoexcited carriers modify the dynamic responses of metamaterials; second, the decay pathway of photoexcited metamaterials after femtosecond (fs) excitation is not explicitly studied, and, particularly, the temporal evolution of the transient states have only been understood as a density-*independent* relaxation back to the equilibrium.

In this paper, we demonstrate an ultrafast reversible modulation of resonant THz absorption in *strongly photoexcited* metamaterials by optical pump and THz probe spectroscopy. This process directly manifests itself via a remarkable re-emergence of the originally quenched THz resonance above a crossover density $N_c \sim 4.7 \times 10^{16}$ cm^{-3} after femtosecond photo-excitation. Increasing the excitation from below to above the transition density, we identify two distinctly different relaxation pathways of the THz resonance with opposite dynamics. A model calculation of transient spectra incorporating the first order diffraction mode from the photo-induced transient grating reproduces the salient features, which is further corroborated by their dependence on the unit cell lattice constant. The revealed scheme represents a relatively simple and generic approach to achieve nonlinear and frequency-agile functions in THz devices without particularly complex structures.

II. EXPERIMENTAL RESULTS

The samples used are double SRRs on GaAs, illustrated as Fig. 1 (a), which are patterned 6 μm copper rings on high resistivity GaAs of 630 μm thick. We mainly focus on two SRR samples with unit cell lattice constant of 50 and 45 μm, and the outer dimension of an individual SRR is 36 μm. Our optical pump and THz probe spectroscopy setup is driven by a 1 kHz Ti:sapphire regenerative amplifier with 40 fs pulse duration at 800 nm. The further details of lasers and experimental setup can be found elsewhere[20]. Shortly, one part of the output is used to excite the sample, while a small fraction is used to generate and detect THz pulses.[21] Phase-locked THz field transients are used as a probe, generated via optical rectification and detected by electro-optic sam-

pling in 1 mm ZnTe crystals (Appendix). Copper apertures of 2.5 mm are placed in front of the sample and a GaAs reference to ensure a uniform illumination and faithful comparison. The THz field transmission coefficient $T(\omega)$ is obtained by the ratio between two Fourier transformed spectra from the transmitted THz probe pulses through the SRRs and bare GaAs. We derive the complex transmission coefficient $T^*(\omega) = |T(\omega)|\, e^{i\phi(\omega)}$, where $|T(\omega)|$and $\phi(\omega)$ are the amplitude and the phase, respectively, by the ratio for the Fourier transformed signals. Transient THz signals are recorded at various time delays with respect to the pump pulse to obtain time-dependent $T(\omega, \Delta\tau)$. The whole setup is purged with dry-N_2 gas.

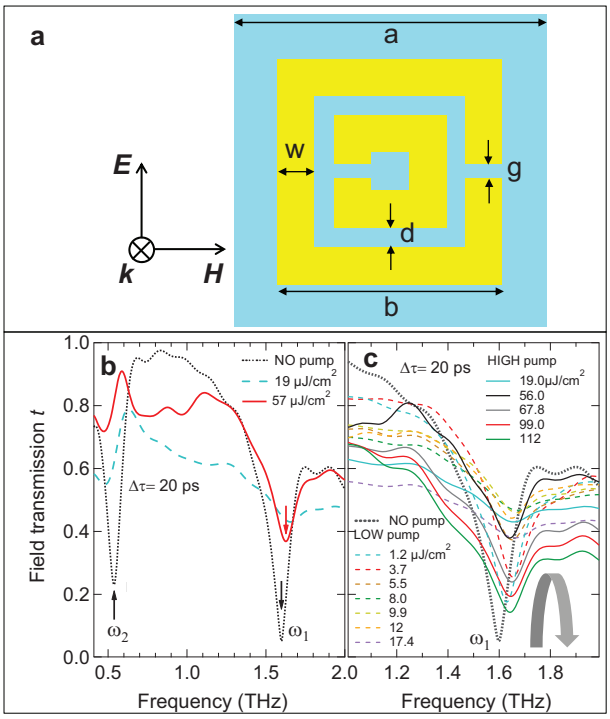

FIG. 1. (color online)(a): Schematic of the SRR unit cell of sample and the polarization of the normally incident THz radiation. a=50 μm, b=36 μm, d=3 μm, g=2 μm, and w=6 μm. (b): Transient transmission spectra $T(\omega)$ taken under two excitation fluences, 19 (cyan dashed) and 57 μJ/cm^2 (red solid), respectively. Static transmission spectra without pump is plotted together (black dotted). (c): The non-monotonic pump fluence dependence (indicated by the gray arrow) of the resonant absorption ~1.63 THz for low (dashed lines) and high (solid lines) photoexcitation. Spectra in both panels are taken at fixed time delay of 20 ps.

The static transmission spectra are shown in Fig. 1(b) (black dotted) with a THz probe normally incident on the sample plane. The E field of the probe is parallel to the gaps of SRRs (see Fig. 1(a)). There are two main THz resonances detected in this configuration at ω_1 ~1.6 and ω_2~ 0.5 THz, which originate from resonant electric processes consistent with prior measurements.[13,18] The ω_1 can be understood as the electric dipole resonance of the metallic bars of the SRRs, and the ω_2 is the magnetic dipole resonance induced by the circulating electric currents generated by the incident E field.

The two THz resonances exhibit distinctly different pump fluence dependence, as shown in the transient THz transmission spectra at $\Delta\tau$ =20 ps (Fig. 1(b)) for two pump fluences: 19 (cyan dashed) and 56 μJ/cm^2 (red solid). The 20 ps time-delay between the excitation and probe pulse is introduced to ensure a measure of quasi-steady state considering the transient carrier lifetime in GaAs on the order of 1 ns. The 19 μJ/cm^2 trace exhibits largely quenched resonances for both ω_1 and ω_2 after photoexcitation. However, the 56 μJ/cm^2 trace clearly shows substantial recovery of the resonant THz absorption around ω_1, while the ω_2 resonance remains quenched. This salient feature is further corroborated in the detailed pump fluence dependence shown in Fig. 1(c). In the low excitation regime from 1.2 to 19 μJ/cm^2, there is a clear weakening in the transition strength and broadening in the linewidth for the ω_1 resonance, with an almost complete quenching at pump fluence of 19 μJ/cm^2. Here, the transmission is ~45% higher and the peak energy has a blue shift of ~60 GHz. In strong contrast, futher increasing photoexcitation from 56 to 112 μJ/cm^2 results in a progressively pronounced resonance. The spectra clearly show a red shift of the resonance energy, ~20 GHz for the highest pump fluence used, a partial recovery of the transition strength and linewidth narrowing. This remarkable non-monotonic behavior and re-emerging resonance near the ω_1 manifest a reversible and frequency-agile modulation of the resonant THz absorption by photoexcitation. This behavior has been seen experimentally for the first time. We explain below that for very high pump fluence, the first-order diffraction will surpass the electric resonance behavior in the THz responses of photoexcited metamaterials. In Fig. 1(c), the dips in the transmission above 56 μJ/cm^2 are due to the first-order diffraction peaks discussed below.

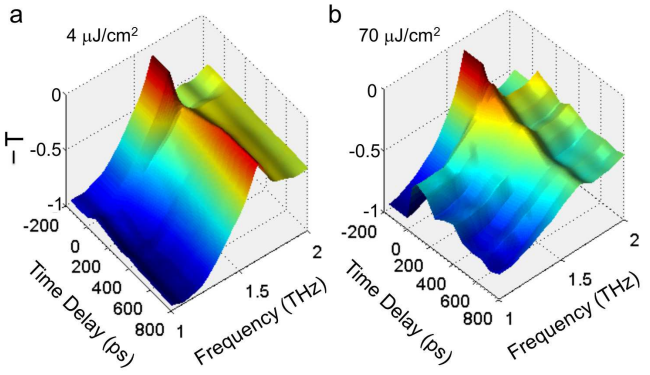

FIG. 2. (color online) Time evolution of negative transmission spectra, $-T(\omega)$, in the photoexcited metamaterial of 50μm lattice constant for (a) 4 and (b) 70 μJ/cm^2, respectively. These clearly show the opposite relaxation pathways for the weak and strong excitation regimes (see text).

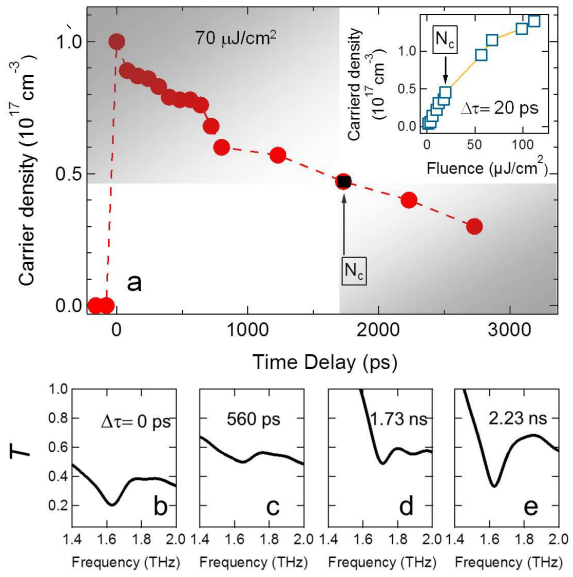

FIG. 3. (color online)(a) The extracted transient carrier concentration as a function of time delay. The left and right gray areas illustrate a crossover from the high to low excitation regime with a crossover density N_c (black square). The inset plots the extracted transient carrier concentration as a function of pump fluence at $\Delta\tau$ =20 ps, marked together with N_c corresponding to the density excited by 19 μJ/cm^2. (b)-(e): The transient transmission spectra T(ω) at various time delays following 70 μJ/cm^2 photoexcitation.

The weak and strong photoexcitations lead to significantly different relaxation pathways back to the equilibrium, as shown in the time evolution of T(ω) spectra following photoexcitation in Figs. 2(a) and 2(b). For pump fluence at 4 μJ/cm^2, the THz absorption $\sim \omega_1$ resonance exhibit an initial photoinduced reduction, immediately followed by a relaxation back to the original value on a ns time scale. Interestingly, opposite to those at the low excitation, the 70 μJ/cm^2 dynamics clearly show a further reduction of the THz resonance ~1.6 THz following the initial decrease. We emphasize two key aspects of this observation: (i) at the large time delay of $\Delta\tau$ =800 ps, the THz resonance ~1.6 THz is almost completely quenched for the 70 μJ/cm^2 excitation, although a clear recovery of the resonance has been seen for the 4 μJ/cm^2 case; and (ii) the pump-fluence-dependent relaxation dynamics of the resonance indicates another way to achieve nonlinear and reversible THz modulation by tuning the time delay.

Ultrafast photoexcitation strongly alters the electronic states in the GaAs substrate by injecting non-equilibrium transient carriers during the pulse duration of 40 fs. Subsequent carrier-carrier/carrier-phonon collisions lead to decoherence and then to a quasi-thermal, hot transient carrier distribution within 1 ps. This hot carrier distribution further cools by emitting phonons and eventually relaxes to the equilibrium by carrier recombination on the order of 1 ns. In the weak excitation regime below 19 μJ/cm^2 (see Fig. 1), the injected carriers make the GaAs regions in the gaps of SRRs and in between them conductive. This leads to the reduction of the resonant absorption near ω_1 and even complete quenching of the resonances.[13] Thus, the observed crossover from the photoinduced quenching to re-emergence of the THz resonance clearly indicates a new collective excitation setting at the high excitation regime not accessible in the previous measurements.

To gain quantitative insights into the transition density N_c for the excitation-induced crossover behavior, we experimentally study the evolution of the transient carrier density under two different strategies: 1) tune the pump fluence with a constant time delay, $\Delta\tau$, and 2) play with the time delay, $\Delta\tau$, by applying a fixed high pump power. The phase-sensitive nature of the time-domain THz field measurement can directly yield both real and imaginary parts of the optical conductivity in the photoexcited GaAs substrate on equal footing without any model assumptions. This provides a direct determination of the transient carrier density, based on an analysis using the Drude model (see Appendix). Referring to the set of measurements in Figs. 1 and 2, we show the fluence-dependent carrier concentration at $\Delta\tau$ = 20 ps in the inset of Fig. 3(a), and the transition occurs at density $N_c = 4.7 \times 10^{16}$ cm^{-3}, which corresponds to pump fluence 19 μJ/cm^2. On the other hand, Fig. 3(a) plots the temporal evolution of the transient carrier concentration excited by 70 μJ/cm^2, which shows an exponential decay with a peak density 10^{17} cm^{-3}. By correlating the temporal profile to the fluence dependence of the carrier density, we define a crossover point at time delay of $\Delta\tau_c$ ~1.73 ns (black square) corresponding to the transition. Here, we mention the transition is not related to the high-reflective/antireflective regime discussed in Ref. 21. Transient spectra at various time delays, as shown in Figs. 3(b)-(e),[23] show a reversal of the THz transmission change once the system is driven across the boundary, corroborating well with our conclusion, e.g., the THz transmission recovers its strength at $\Delta\tau$ =2.2 ns after initial quenching at time delays before 1.73 ns.

III. SIMULATIONS AND DISCUSSIONS

Next, we analyze the transient THz response of photoexcited metamaterials by full-wave numerical simulations. First, we take into account the photoexcitation-induced dynamic response of the GaAs substrate. In our simulations, for simplicity we only consider a 1-μm-thick homogeneously photo-modulated layer described by the well-established Drude model beneath the copper SRRs, but neglect the un-modulated regions hidden by SRRs in the optical path. (We have checked and determined it has little influence on the results.) The settings in the simulations describe the experiments, in which the two ports are settled in a vacuum at the two sides of the SRR-sample, as the source and receiver ports (see Fig.

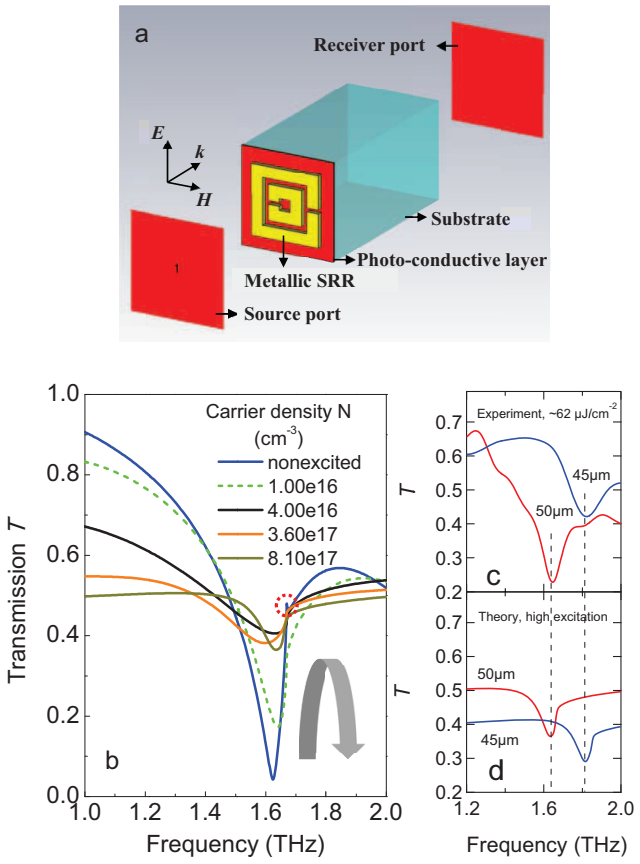

FIG. 4. (color online) (a): Schematic of the simulation configuration. (b): The simulated THz transmission spectra for various carrier densities, N; The dotted circle shows a tiny kink, the feature of the first-order diffraction, for the unpumped case. The photoinduced THz resonances in the strong excitation regime for two different lattice constants 45 and 50 μm: (c) experiment and (d) simulation.

4(a)). A time filter has been used to gate out the echo signals from the multi-reflection, the same as the time windowing in the experiments. The frequency-dependent complex conductivity of the Drude model for the photoexcited layer is $\sigma = \varepsilon_0\omega_p^2/(\gamma - i\omega)$. Here, ε_0 is the permittivity of a vacuum, γ represents the collision frequency, and $\omega_p = \sqrt{Ne^2/(\varepsilon_0 m^*)}$ the plasma frequency. The free electron charge e is 1.6×10^{-19}C and the effective carrier mass in GaAs, $m^* = 0.067m_0$ (m_0, the mass of a free electron). We modulate the carrier density N in our simulations. Thus, the photoexcited layer has the dielectric function, $\varepsilon(\omega) = \varepsilon_s + i\sigma/(\varepsilon_0\omega)$, where ε_s (=12.7) is the dielectric constant of the undoped GaAs substrate. In our simulations, we keep $\gamma = 1.8$ THz for all the cases as in Ref. 18.

Figure 4(b) shows the simulated transmission spectra for various carrier densities N. The simulation clearly shows the crossover from a reduction to an enhancement of the resonant THz absorption ~1.6 THz as the excitation from low to high density regimes. This agrees well with the photoinduced reversible modulation demonstrated in the experiments. Specifically, in the low density below 4.0×10^{16} cm^{-3}, the THz resonance peak in the transmission curve exhibits clearly weakened transition strength, a blue-shift and spectral broadening. Increasing the carrier density above 4.0×10^{16} cm^{-3}, the resonant THz peak progressively reemerges, e.g., a clear transmission dip seen for the case $N = 8.1 \times 10^{17}$ cm^{-3}. From the simulations, we can attribute the reemergence of the resonant THz absorption at high density to the effect of first-order diffractive waves from photoinduced transient grating. Due to the periodic structure of the SRRs, the first-order diffractive wave is determined to propagate in the substrate at high excitation, which strongly influences the fundamental absorption mode. This leads to a new THz transmission dip at $f_1 = c/(na)$ above a transition density $\sim 4.0 \times 10^{16}$ cm^{-3}. Here, c is light speed in a vacuum, n the refractive index of GaAs, and a the lattice constant of the structure. The SRR structure with the dipole resonance close to f_1 allows achieving a reversal of resonant THz absorption with increasing photoexcitation, due to a crossover in the absorption from the dipole mode to the diffraction mode.

In the photoexcited states, the resonance ~1.6 THz will be influenced by both electrical dipole resonance and the first order diffraction, due to photoinduced grating. Both show strong excitation fluence dependence, whose interplay leads to the observed reappearance of the THz resonance. Regarding the contribution from the first order diffraction, it indeed exists regardless of the excitation fluence. However, the efficiency of the diffraction should strongly depend on the excitation fluence because the index contrast is a strong and nonlinear function of the photo-injected carrier density. In the low fluence regime, the first order diffraction is relative inefficient and produces smaller scattering intensity than from the photo-induced softening of electrical dipole resonance. Consequently, the net effect is the decrease of the amplitude of the THz resonance. However, the opposite behavior appears at high photo-excitation. Here, the electrical dipole resonance is strongly quenched and the response is dominated by first-order diffraction contributions. The diffraction peak becomes more pronounced at high pump fluence. Thus, referring to the cross-over point in Fig. 3a, we can attribute this to a transition between two regimes, where the first (low fluence) is dominated by electrical dipole absorption in metamaterials, and the second (high fluence) by first order diffraction. Additionally, if we have a careful look at the simulation results for the unpumped case in Fig. 4b, we may find a feature of a tiny kink (marked with the dotted circle) at the frequency corresponding to the first-order diffraction. Such a feature finally becomes a dip under high fluence.

To corroborate our model, we compare the re-emerged THz resonances from the experiment (Fig. 4(c)) to those from the simulation (Fig. 4(d)) for two different lattice constants, 50 and 45 μm, respectively. The simulations are performed on the structures with the

same double-SRR array for the case with the density $N = 8.1 \times 10^{17}$ cm^{-3}. It is clearly visible that the simulated transmission dip to higher frequency by decreasing the lattice constant and the dip positions tightly link to the frequency of the first-order diffraction mode for each case. An extremely good agreement between the simulation and the experiment is found for the transmission-dip position and its shift, which underpins the effect of the first-order diffraction mode in the strongly excited metamaterials.

IV. CONCLUSIONS

In summary, we have demonstrated ultrafast photoinduced reversible modulation of resonant THz absorption in strongly photoexcited metamaterials. Increasing the excitation from below to above the threshold density, N_c, we observe a crossover from a complete quenching to a re-emergence of the THz resonance. Our analysis and theoretical simulations, based on the first order propagation from the photoinduced transient grating, explain the density- and lattice-constant-dependent frequency shifts. Our results clearly identify the importance of photoinduced optical modes in metamaterials, besides the electronic resonances, which should be carefully considered in designing future multifunctioning photonic-electronic devices using the artificial periodical structures. The easy implementation of the revealed scheme represents another approach to achieve nonlinear and frequency-agile functions in THz devices.

Work at Ames Laboratory was supported by the Department of Energy (Basic Energy Sciences) under contract No. DE-AC02-07CH11358. This was partially supported by the IC Postdoctoral Fellowship Program.

APPENDIX

To quantitatively simulate the experimental results, we determine temporal evolution of the THz conductivity in the photo-excited GaAs substrate. The phase-sensitive nature of the time-domain THz field measurement can directly yield both real and imaginary parts of the optical conductivity on equal footing without any model assumptions. Particularly, it is more transparent to express the THz response of the sample as $\sigma(\omega) = \sigma_1(\omega) + i\omega\epsilon_0(1 - \epsilon_1(\omega))$, where $\sigma_1(\omega)$ denotes the conductive, absorbed power density, while $\epsilon_1(\omega)$ describes the dispersive, out-of-phase response.

After photoexcitation, complex-valued $\sigma(\omega)$ transient changes to the modified value $\sigma(\omega) + \Delta\sigma(\omega)$, where $\Delta\sigma(\omega)$ is due to the photo-induced changes. We experimentally determine $\Delta\sigma(\omega)$ at pump-probe time delay, $\Delta\tau$, by measuring the transmitted THz reference field in equilibrium and the pump-induced change. Figure 5(a) plots the pump induced ΔE_{THz}(t) (red) at 2.73 ns after photoexcitaiton and reference THz field E_{THz}(t)

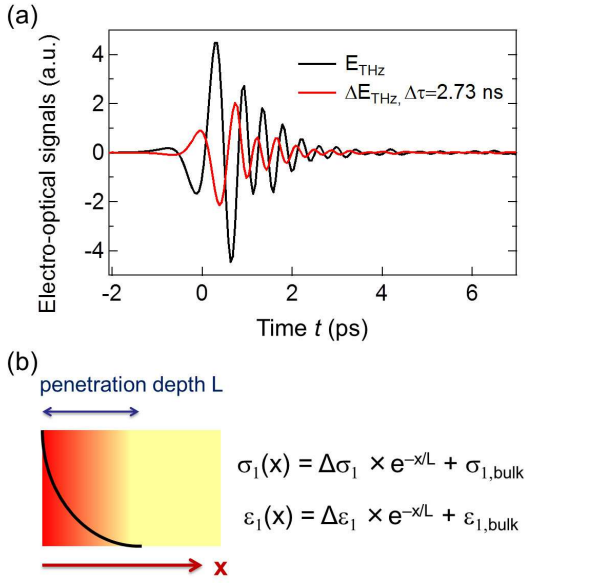

FIG. 5. (color online) (a) Pump induced changes ΔE_{THz} (red) at $\Delta\tau$ =2.73 ns and reference THz fields E_{THz} (black). (b) The exponential decay of the excited carriers with the penetration depth of the pump pulse in the GaAs sample. This has been taken into account in the numerical analysis as illustrated (see text for details).

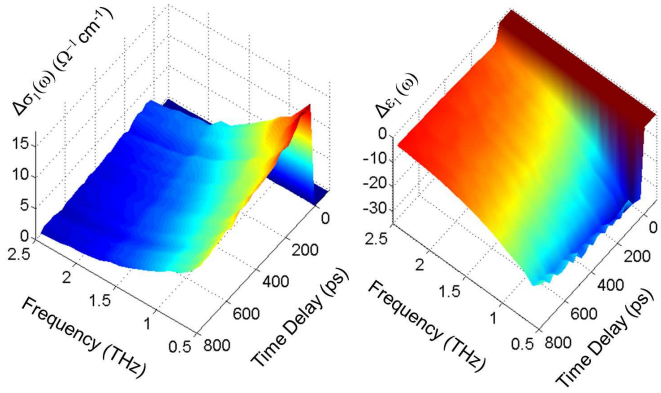

FIG. 6. (color online) Photoinduced conductivity change $\Delta\sigma_1(\omega)$ (a) and dielectric function change $\Delta\epsilon_1(\omega)$, (b) in GaAs is photoexcited by a near-infrared (800 nm) laser pulse of 40 fs duration. The response is shown for pump-probe delays $\Delta\tau$ and frequency. Note, the phase-resolved THz E-field is obtained directly in the time domain and used to analyze complex-valued response functions without Kramers-Kronig transformation (see text).

(black). Fourier transformation then yields the complex-valued transmission function, $T^*(\omega) = [E_{\mathrm{THz}}(\omega) + \Delta E_{\mathrm{THz}}(\omega)]/E_{\mathrm{THz}}(\omega)$. Subsequently, we calculated the transmission function using transfer matrix formalism, based on Fresnel equations in the thin film limit, which yields $T^* = f(\sigma(\omega), \Delta\sigma(\omega))$. Critical to note is the exponential decay of the excitation density in the material,

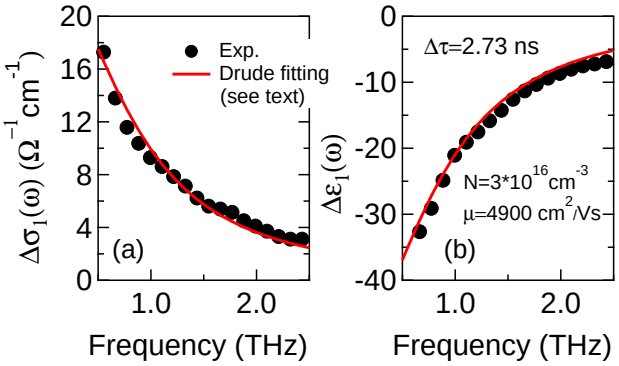

FIG. 7. (color online) The induced conductivity $\Delta\sigma_1(\omega)$ (a) and dielectric function $\Delta\epsilon_1(\omega)$, (b) measured at time delay, $\Delta\tau$ =2.73 ns. Solid lines calculated THz response, using the Drude model for density 3×10^{16} cm^{-3} and mobility $\sim$ 4900 cm^{-2}/Vs.

as illustrated in Fig. 5(b). We have taken this into account in the numerical analysis by dividing the sample into many thin slabs, each has a uniform carrier concentration. Finally, we iteratively fit $\sigma_1(\omega)$ and $\epsilon_1(\omega)$ to the measured transmission function $T^*(\omega)$ at the fixed time delay, which allows obtaining both temporal and spectral responses of $\Delta\sigma_1$ and $\Delta\epsilon_1$. Figures 6(a) and 6(b) show the extracted frequency-dependent complex THz conductivity as the function of time delay in photoexcited GaAs. Here, a strongly negative $\Delta\epsilon_1(\omega)$ and large low-frequency conductivity follow closely the Drude model, as seen in the solid lines in Figs. 7(a) and 7(b). Such analysis provides a direct experimental determination of the transient carrier density shown in Fig. 3(a) in the main text. For instance, the electron mobility, μ, and transient carrier density at $\Delta\tau$ =2.7 ns are 4900 cm^{-2}/Vs and 3×10^{16} cm^{-3}, respectively, (Fig.3) from our analysis, in good agreement with the literature.[24]

* jwang@ameslab.gov, jgwang@iastate.edu
† nhshen@ameslab.gov
‡ Present address: Department of Physics, University of South Florida, Tampa, FL

[1] D. R. Smith, J. B. Pendry and M. C. K. Wiltshire, Science **305**, 788 (2004).
[2] C. M. Soukoulis, S. Linden, and M. Wegener, Science **315**, 47 (2007).
[3] V. M. Shalaev, Nature Photon. **1**, 41 (2007).
[4] C. M. Soukoulis and M. Wegener, Nature Photon. **5**, 523 (2011).
[5] R. A. Shelby, D. R. Smith, S. Shuldtz Science **7**, 292 (2001).
[6] T. J. Yen, et al., Science **303**, 1494 (2004).
[7] S. Linden *et al.*, Science **306**, 1351 (2004).
[8] N. Fang, H. Lee, C. Sun, and X. Zhang, Science **308**, 534 (2005).
[9] J. B. Pendry, Phys. Rev. Lett. **85**, 3966 (2000).
[10] S. Zhang *et al.*, Phys. Rev. Lett. **95**, 137404 (2005).
[11] A. K. Azad, J. Dai, and W. Zhang, Opt. Lett. **31**, 634 (2006).
[12] H. T. Chen, W. J. Padilla, J. M. O. Zide, A. C. Gossard, A. J. Taylor, and R. D. Averitt, Nature **444**, 597 (2006).
[13] W. J. Padilla, A. J. Taylor, C. Highstrete, M. Lee, and R. D. Averitt, Phys. Rev. Lett. **96**, 107401 (2006).
[14] N. H. Shen *et al.* Phys. Rev. Lett. **106**, 037403 (2011).
[15] H. T. Chen *et al.*, W. J. Padilla, J. M. O. Zide, S. R. Bank, A. C. Gossard, A. J. Taylor, and R. D. Averitt, Opt. Lett. **32**, 1620 (2007).
[16] H. T. Chen *et al.*, J. F. O'Hara, A. K. Azad, A. J. Taylor, R. D. Averitt, D. B. Shrekenhamer, and W. J. Padilla, Nature Photon. **2**, 295 (2008).
[17] H. T. Chen *et al.*, Phys. Rev. Lett. **105**, 247402 (2011).
[18] J. M. Manceau, N. H. Shen, M. Kafesaki, C. M.Soukoulis, and S. Tzortzakis, Appl. Phys. Lett. **96**, 021111 (2010).
[19] K. M. Dani *et al.*, Nano Lett. **9**, 3565 (2009)
[20] T. Li *et al.*, Phys. Rev. Lett. **108**, 167401 (2012); J. Wang *et al.*, Phys. Rev. Lett. **104**, 177401 (2010); J. Wang et al.,Phys. Rev. B **77**, 235308 (2008).
[21] Q. Wu and X.-C. Zhang, Appl. Phys. Lett.**68**, 1604 (1996).
[22] L. Fekete, J. Y. Hlinka, F. Kadlec, P. Kužel, and P. Mounaix, Opt. Lett. **30**, 1992 (2005).
[23] Note, the transmittance presented in the paper is relative values by comparing transmitted signals from the photoexcited metamaterial sample and those from a photoexcited reference substrate (bare GaAs). This should not be confused with the absolute transmittance from the sample. Consequently, the THz transmission through the photoexcited GaAs is suppressed across the entire THz spectrum measured, due to the free carrier Drude conductivity. However, in the case of metamaterials, the changes are mostly pronounced near the dipole resonances. At spectral positions away from the resonances, the ratio between the two could be larger than 1. Note, this effect should not affect the transition energy shift and spectral width discussed, but rather can be thought as adding a feature-less offset to the transient spectrum.
[24] Matthew C. Beard, Gordon M. Turner, and Charles A. Schmuttenmaer, Phys. Rev. B **62**, 1576 (2000).